Strong coupling effects in $(\text{Nb-Al-AlO}_x)_2$-Nb stacked Josephson junctions

E. Goldobin,* M. Yu. Kupriyanov,† I. P. Nevirkovets,‡ A. V. Ustinov,§ M. G. Blamire,‖ and J. E. Evetts‖
Institute of Thin Film and Ion Technology (ISI), Research Center Jülich GmbH (FZJ), D-52425 Jülich, Germany
(Received 13 July 1998)

Stacked $(\text{Nb-Al-AlO}_x)_2$-Nb long Josephson junctions with very thin intermediate Nb-Al superconducting layer are investigated experimentally and theoretically. Stable coherent in-phase zero-field steps (ZFS's) are observed; both the critical current and the maximum ZFS current dependence on magnetic field are measured to prove the in-phase nature of this mode. The dependences are in good agreement with the inductive coupling model. The Swihart velocities for in-phase ($\overline{c}_+$) and antiphase ($\overline{c}_-$) modes are measured for different lengths of the stacks. In order to make a proper interpretation of the experimental results, an extension of the existing model is developed, taking into account the fact that the middle electrode consists of two different superconductors (Nb and proximized Al). A comparison of a new model with the conventional model and experimental data is made. The extended model gives the $\overline{c}_+/\overline{c}_-$ ratio as 30% different from what the conventional model predicts. For thin Nb and Al layers the correction factor depends only on the ratio of the magnetic field penetration depths in Nb and proximized Al. [S0163-1829(98)04746-8]

I. INTRODUCTION

Stacked long Josephson junctions (LJJ's) have recently received much attention. They show a variety of new physical phenomena[1–4] in comparison to that found in single junctions and have potential for applications.[5–8] In addition, the naturally layered high-T_c superconductors (HTS's) can be described as intrinsic stacks of Josephson junctions.[9]

The dimensionless coupling constant S $(-1<S<0)$ which defines the strength of the inductive interaction between the junctions depends on the thickness d of their common superconducting electrode and its London penetration depths λ. For the case of a symmetric twofold stack, S can be calculated using the following expression:[10]

$$S=\frac{s_m}{d'}, \tag{1}$$

where

$$s_m=\frac{-\lambda_m}{\sinh(d_m/\lambda_m)}, \tag{2}$$

and

$$d'=\lambda_m\coth(d_m/\lambda_m)+\lambda\coth\left(\frac{d}{\lambda}\right) \tag{3}$$

are the constants which characterize the relative thickness of the middle electrode and the effective magnetic thickness, respectively. Here $d_{a,b,m}$ and $\lambda_{a,b,m}$ are the thicknesses and the London penetration depths of the top, bottom, and middle superconducting layers, respectively. Equation (1) assumes that the stack is symmetric, i.e., $d_a=d_b=d$ and $\lambda_a=\lambda_b=\lambda$. A more general expression for the asymmetric case can be found in Ref. 11. The coupling increases with decreasing of the thickness d_m of the middle electrode.

For the high-T_c intrinsic stacks, the coupling S between JJ's is very strong due to small thickness d of the superconducting Cu-O layers which is of atomic scale,[9] much smaller than the London penetration depth λ. In contrast, for artificially prepared low-T_c $(\text{Nb-Al-AlO}_x)_N$-Nb stacks studied so far,[1–4,12] the coupling was weak or moderate since the thickness of common superconducting electrodes was typically of the order of λ. Thus, in order to bridge our understanding from low-T_c stacks to their high-T_c counterparts it is rather interesting to study low-T_c stacks with the thickness of superconducting layers of the order of the coherence length ξ which is much smaller than λ. This condition is possible to realize in the artificially prepared $(\text{Nb-Al-AlO}_x)_N$-Nb stacks. As a model system to study strong coupling effects, we use $(\text{Nb-Al-AlO}_x)_2$-Nb stacks with the thickness of the intermediate layer d_m being much smaller than its London penetration depth λ_m. This limit allows us to check the relevance of the inductive coupling model[10] used so far to describe intrinsic multilayers. Other coupling mechanisms, if any, may be revealed from such a comparison.

One of the important features of N-fold stacked long JJ's is the presence of N modes of electromagnetic plasma waves and, accordingly, N characteristic (Swihart) velocities. The Swihart velocity[13] in single long JJ is defined as a minimum phase velocity of linear plasma waves in the system, $\overline{c}_0=\min[\omega(k)/k]$ for all k, and can be calculated as

$$\overline{c}_0=\lim_{k\to\infty}\frac{\omega(k)}{k}. \tag{4}$$

Two coupled LJJ's have two Swihart velocities denoted as $\overline{c}_+$ and $\overline{c}_-$ and defined as in Eq. (4) but with dispersion relations $\omega_+(k)$ and $\omega_-(k)$ corresponding to two different branches: in-phase one and out-of-phase one.[3,14]

For a symmetric twofold stack, the characteristic velocities $\overline{c}_+$ and $\overline{c}_-$ can be expressed via the Swihart velocity of a single junction $\overline{c}_0$ with the same parameters as

$$\overline{c}_\pm=\frac{\overline{c}_0}{\sqrt{1\pm S}}. \tag{5}$$

Sakai *et al.*[10] considered theoretically the static and dynamic properties of fluxons. When one fluxon is trapped in each junction of the twofold stack, two distinct fluxon modes were found: the ''symmetric'' and the ''coherent'' (in-phase) mode. These modes were calculated as stable dynamic states which account for the so-called zero-field steps (ZFS's) on the I-V characteristic (IVC) of the stack. For the coherent mode, which has the Swihart velocity $\overline{c}_+$, there is no phase shift between the fluxons. In spite of an early prediction by Sakai *et al.*,[10] the in-phase fluxon mode was found to be unstable in most of the experiments reported so far, and remained practically not investigated experimentally. At the same time, this mode is apparently the most interesting for applications due to coherent phase oscillations in two LJJ's.

Monaco *et al.*[15] observed ZFS's in a double-junction stack and interpreted one of the steps as the in-phase ZFS. However, no experimental data about the dependence of the height of this step on the length and on applied magnetic field were obtained. In addition, the measured values of the velocities $\overline{c}_+$ and $\overline{c}_-$ were not in agreement with the theory.[10]

Strong coupling between JJ's may improve the stability of the in-phase fluxon state, i.e., when two fluxons (one in each JJ) move synchronously and have the same coordinate and speed. Since the middle electrode is thin, its inductance is rather high and it is more favorable energetically to have a fluxon configuration in which the screening currents of fluxons in the middle electrode cancel each other (in-phase state). Grønbech-Jensen *et al.*[16] showed analytically that in spite of repulsion between two fluxons in statics, the in-phase state becomes stable at high velocity.

In this paper we prove this prediction experimentally. We present experimental evidence of the in-phase ZFS mode in very strongly coupled double-barrier (Nb-Al-AlO$_x$)$_2$-Nb stacks consisting of high-quality Josephson tunnel junctions with nearly identical critical current densities. Numerical simulations of the dependence of the ZFS maximum current on magnetic field are performed and compared with the experimental data. The ratio $\overline{c}_+/\overline{c}_-$ is measured experimentally from the voltage spacing of in-phase ZFS's and antiphase FS's for different lengths of the stack. An extension of the model[10] is developed to account for the very thin Nb-Al bilayer in the middle electrode with suppressed energy gap. The comparison of the experimentally measured $\overline{c}_+/\overline{c}_-$ ratio with the extended theory is given.

II. SAMPLES AND EXPERIMENTAL SETUP

The sample fabrication route, in general, follows that described in Ref. 17. The double-barrier (Nb-Al-AlO$_x$)$_2$-Nb structures were fabricated on sapphire R-plane substrates by a whole-wafer process in ultrahigh vacuum. Both Nb and Al films were deposited using dc magnetron sputtering. The thicknesses of the bottom, middle, and top (not including wiring layer) Nb films are 150 nm, 7 nm, and 100 nm, respectively. The thickness of the Al films, as deposited, is 6.5 nm. Thus, the middle electrode is a Nb-Al bilayer with approximately equal thickness of Nb and Al. The sample geometry is shown schematically in Fig. 1. Stacks of four different lengths $L=20, 40, 60,$ and $80\ \mu$m were investigated. The width of each device was about $W\approx 12\ \mu$m. The critical current density of the junctions was $j_c\approx 420 \pm 36$ A/cm^2 ($\pm 8.6\%$). The spread was measured among eight JJ's fabricated on the same substrate. The magnetic field was applied in the plane of the tunnel barriers and perpendicular to the larger dimension L of the devices. Two stacked junctions were always measured in series, without a contact to the middle electrode.

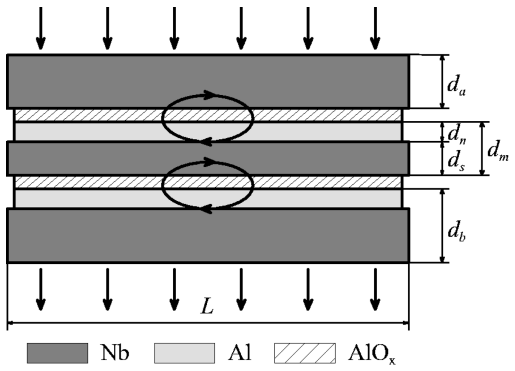

FIG. 1. Schematic view of the junction geometry: $d_{a,b,m}$ are the thicknesses of the top, bottom, and middle electrodes: $d_{n,s}$ are the thicknesses of the Al and Nb films in the middle superconducting electrode, respectively.

III. EXPERIMENTAL RESULTS

The IVC of the stack with $L=40\ \mu$m at $T=4.2$ K is shown in Fig. 2. A plot is obtained for zero applied magnetic field, $H=0$. In the region $H \ll H_{c1}$ the device reveals the current locking behavior[4] manifested by switching from the critical current I_c at zero voltage to the double-gap voltage $V_g^{\Sigma}=(\Delta_a+\Delta_b+2\Delta_m)/e$. Here $\Delta_{a,b,m}$ are the energy gaps of the top, bottom, and middle superconducting electrodes, respectively. The gap sum voltage $V_g^{\Sigma}=4.7$ mV is smaller than in stacks with thick, high-quality Nb electrodes, where its typical value is 5.3–5.4 mV. This results from the suppressed Δ_m of the very thin ($d\sim\xi$) middle Nb-Al superconducting

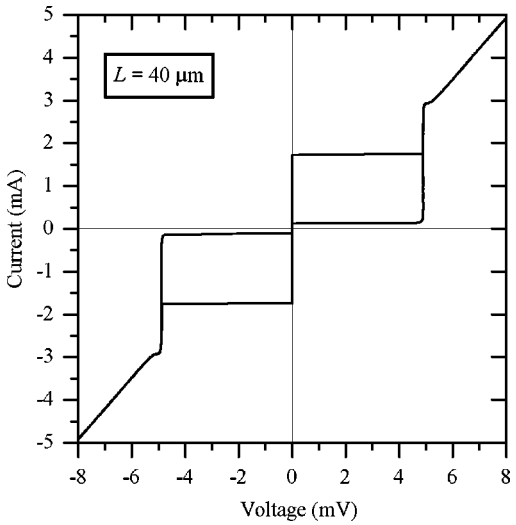

FIG. 2. IVC of the device with $L\times W=40\times 12\ \mu$m^2 at $T=4.2$ K.

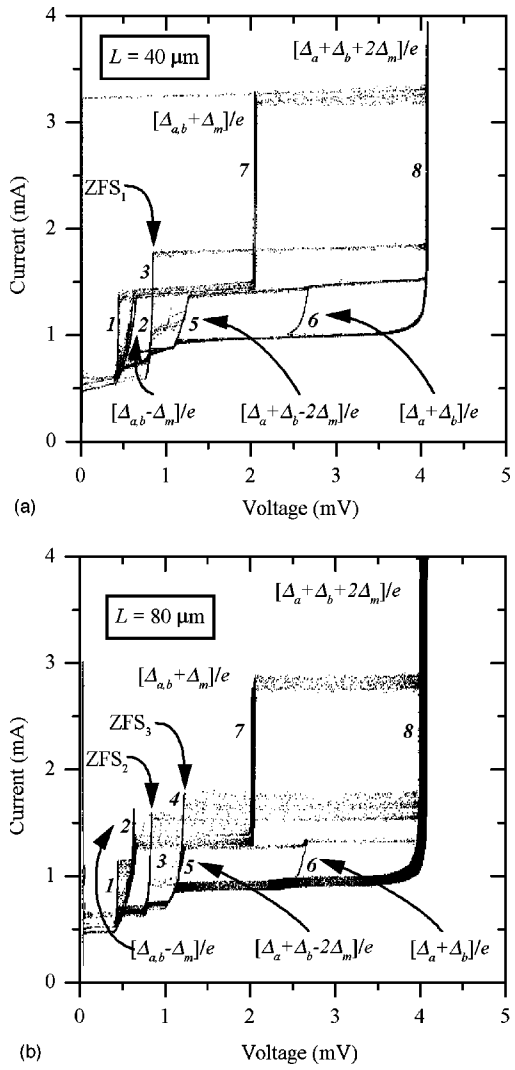

FIG. 3. IVC of the stack with $L=40\ \mu$m (a) and $L=80\ \mu$m (b).

layer. Choosing the proper dc offset, we were able to observe a current step (not shown in Fig. 2) at the voltage $V \approx 2.3$ mV which corresponds to the gap voltage of one JJ, $V_g^{a,b}=(\Delta_{a,b}+\Delta_m)/e$. The critical currents of the JJ's were almost identical and their difference was less than 6%. High subgap resistance was provided by a good quality tunnel barrier. Very similar IVC's were found for other measured stacks with $L=20$, 60, and 80 μm. Thus, all measured samples were high-quality stacked JJ's with almost equal critical currents and suppressed energy gap Δ_m of the middle Nb-Al electrode.

We have not observed any ZFS's at $T=4.2$ K. For all stacks, by increasing the temperature, we were able to observe a set of large and stable steps on the IVC. Examples are shown in Fig. 3(a) for $L=40\ \mu$m and Fig. 3(b) for $L=80\ \mu$m. We investigated the magnetic field dependence of the maximum current of each step. The amplitudes of steps 2, 5, 6, 7, and 8 were not sensitive to the applied magnetic field H. Steps 3 and 4 [step 4 is not present in Fig. 3(a)] had the maximum amplitude at $H=0$, while step 1 had the minimum amplitude at $H=0$. Steps 7 and 8 have been discussed above and are related to the sum of the energy gaps of superconducting electrodes forming the JJ's. One can see that step 7 actually consists of two different branches. The voltages of these branches are $(\Delta_a+\Delta_m)/e$ and $(\Delta_b+\Delta_m)/e$ and the difference between them is equal to $|\Delta_a-\Delta_b|/e$ and related to the small difference in energy gaps of top and bottom electrodes. Since this value is rather small ($\sim 20\ \mu$V), from now on, we assume that in our stacks $\Delta_a=\Delta_b=\Delta_{a,b}$.

Now, let us discuss steps 5 and 6. From the top of these steps the system switches to the gap sum voltage of the whole stack (steps $5\rightarrow 8$, $6\rightarrow 8$, or $5\rightarrow 6\rightarrow 8$); so we can conclude that both JJ's play a role in forming these steps. The amplitude of the steps does not depend on the magnetic field and these steps most likely represent the gap difference feature.

It is well known that if a single tunnel superconductor-insulator-superconductor (S-I-S) JJ has electrodes with different energy gaps Δ_1 and Δ_2, its IVC reveals two steps at voltages $|\Delta_1-\Delta_2|/e$ and $(\Delta_1+\Delta_2)/e$. In the symmetric JJ $(\Delta_1=\Delta_2)$ only the second step is observed. Considering a stack of two asymmetric JJ's connected in series (S_b-I-S_m-I-S_a) and assuming that, at a given current, each JJ is in one of the above two states, one gets four possible voltage combinations across the whole structure:

$$\frac{(\Delta_a-\Delta_m)}{e}+\frac{(\Delta_b-\Delta_m)}{e}=\frac{(\Delta_a+\Delta_b-2\Delta_m)}{e}, \tag{6}$$

$$\frac{(\Delta_a-\Delta_m)}{e}+\frac{(\Delta_b+\Delta_m)}{e}=\frac{(\Delta_a+\Delta_b)}{e}, \tag{7}$$

$$\frac{(\Delta_a+\Delta_m)}{e}+\frac{(\Delta_b-\Delta_m)}{e}=\frac{(\Delta_a+\Delta_b)}{e}, \tag{8}$$

$$\frac{(\Delta_a+\Delta_m)}{e}+\frac{(\Delta_b+\Delta_m)}{e}=\frac{(\Delta_a+\Delta_b+2\Delta_m)}{e}. \tag{9}$$

Two of them, Eqs. (7) and (8), coincide; so we end up with three possible voltages for the steps. The voltage given by Eq. (9) corresponds to the gap sum voltage of the whole stack, i.e., step 8 in Fig. 3; the voltage given by Eq. (6) corresponds to step 5 in Fig. 3; and the voltage given by Eq. (7) or (8) corresponds to step 6 in Fig. 3. To check this point more precisely we traced steps 5, 6, and 8 on the IVC while increasing the temperature. The result is shown in Fig. 4. Making a comparison with Fig. 3 we see that the voltage of step 5 increases and that of steps 6 and 8 decreases with temperature until all of them become equal at some temperature T_c^m. From Eqs. (6)–(9) it comes out that such a situation corresponds to $\Delta_m(T_c^m)=0$; i.e., T_c^m is a critical temperature of the middle Nb-Al superconducting electrode. Step 3 in Fig. 4 was present only at low temperature and disappeared with increasing the temperature.

Normally, steps corresponding to the gap difference feature are not so large. Theory gives a logarithmic divergence of the step amplitude at the voltage near to the gap difference voltage. In experiment, the amplitude of the step (in current) is finite and depends mainly on temperature — the closer to the critical temperature of one of the electrodes, the higher is the step. The gap difference feature may be very weak or even absent in junctions with substantial leakage (non tunnel) currents. Therefore, the large amplitude of these steps in our case and the presence of hysteresis around them are additional signs of the high quality of our junctions.

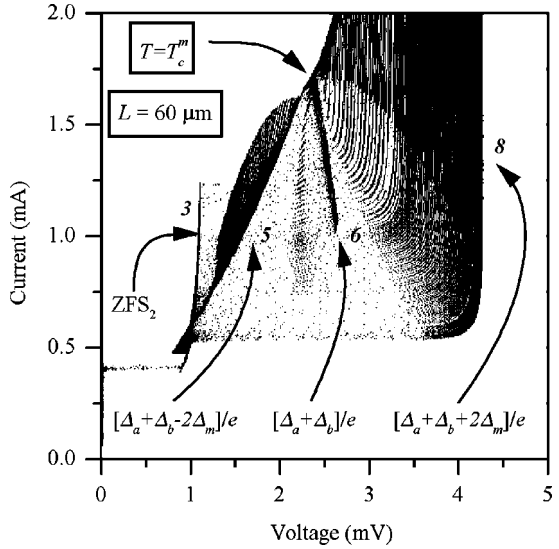

FIG. 4. IVC family which shows the dependence of the gap features on the temperature. At some temperature T_c^m, the voltages of all three steps coincide, so that the SISIS junction becomes a SINIS one.

Step 2 in Fig. 3 corresponds to the voltage state of a single JJ. From the top of this step the device switches to the gap sum voltage state of the individual JJ (step 7). The voltage of step 2 is about half of that of step 5, which gives $V_2=(\Delta_{a,b}-\Delta_m)/e$. One can see that step 2 actually consists of two steps with a difference in voltage $|\Delta_a-\Delta_b|/e$ which is similar to the splitting of step 7. Step 1 is also related to the activity of one JJ because the system switches to step 2 from the top of step 1. The character of the $I_{\max}(H)$ dependence of step 1 lets us assume that this is an in-phase Fiske step of a single JJ. We will not consider steps 1 and 2 in the further discussion because they represent single JJ behavior rather than behavior of the whole stack.

From the top of steps 3 and 4 the stack switches to the gap sum voltage of the whole structure. The amplitude of these steps depends on the magnetic field, having the maximum value at $H=0$. Thus, we conclude that these are synchronized ZFS's of both JJ's. The dependence of the amplitude of these steps on the magnetic field is shown in Fig. 5(a) for $L=80\ \mu$m and Fig. 5(b) for $L=40\ \mu$m. Similar behavior was found for the $L=60\ \mu$m stack. The dependences resemble the conventional $I_{\max}^{\mathrm{ZFS}}(H)$ curve for a single long JJ. This is expected for the in-phase mode where coupled sine-Gordon equations with identical solutions in two junctions are reduced to a single sine-Gordon equation with renormalized Josephson length $\lambda_J^+=\lambda_J/\sqrt{1+S}$. The dependences $I_{\max}^{\mathrm{ZFS}_{2,3}}(H)$ in Fig. 5(a) cannot be traced below some threshold current. From Fig. 3(b) it is clear that magnetic field cannot suppress ZFS$_2$ below the quasiparticle (McCumber) branch of the IVC, i.e., below about 0.75 mA, which exactly coincides with the lowest traceable current in Fig. 5(a). ZFS$_3$ in Fig. 3(b) cannot be suppressed below the top of step 5 (which is independent on H) because they are so close in voltage that it is impossible to distinguish them at high magnetic field H. As a result, the lowest measured current $I_{\max}^{\mathrm{ZFS}_3}(H)$ in Fig. 5(a) is the current corresponding to the top of step 5 in Fig. 3(b) and is about 1.25 mA, which is in good

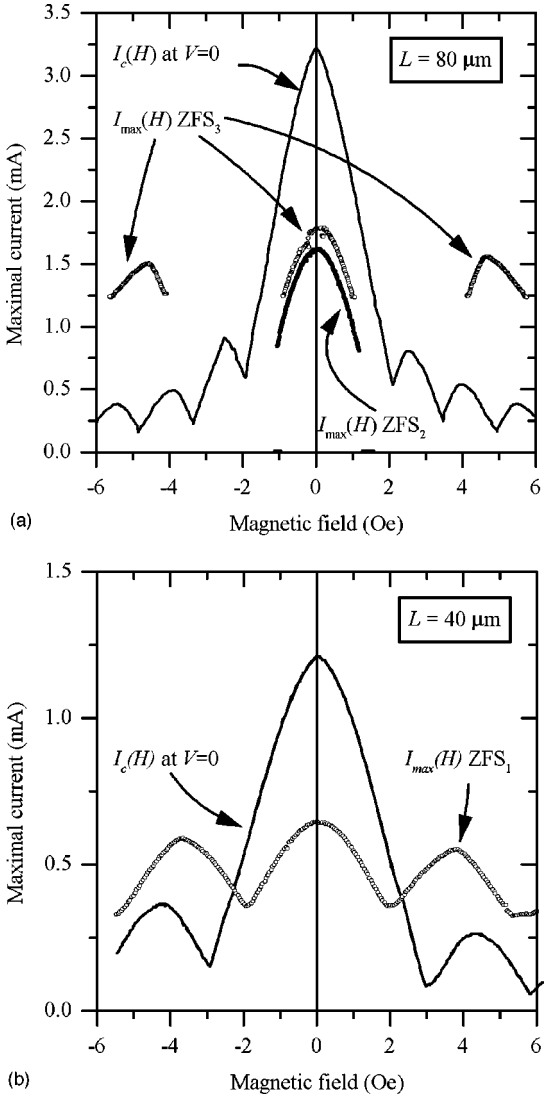

FIG. 5. The dependence of the maximum ZFS current on the magnetic field for (a) $L=80\ \mu$m [$I_{\max}^{\mathrm{ZFS2}}(H)$, $I_{\max}^{\mathrm{ZFS3}}(H)$, and $I_c(H)$ are shown] and for (b) $L=40\ \mu$m [$I_{\max}^{\mathrm{ZFS1}}(H)$ and $I_c(H)$ are shown].

agreement with Fig. 5(a). If the voltage separation of steps 4 and 5 in Fig. 3(b) exceeds the noise level of the experimental system, $I_{\max}^{\mathrm{ZFS}_3}(H)$ in Fig. 5(a) could be *in principle* traced down to the quasiparticle branch (0.85 mA).

The stack of the length $L=20\ \mu$m showed tiny steps 1 and 3 that, nevertheless, were dependent on magnetic field H. This behavior is rather typical for a JJ of normalized length (in in-phase $\overline{c_+}$ mode)

$$\ell^+=\frac{L}{\lambda_J^+}=\frac{L}{\lambda_J}\sqrt{1+S}\approx 1.1. \tag{10}$$

To calculate Eq. (10) we took the value of

$$\lambda_J=\sqrt{\frac{\Phi_0}{2\pi\mu_0 j_c d'}}=4.0\pm 0.2\ \mu\mathrm{m}\ (\pm 5\%), \tag{11}$$

with critical current density given in Sec. II and d' calculated using Eq. (3) with λ_m given by Eq. (34). The coupling parameter S in Eq. (10) was taken from Eq. (19). Due to the

TABLE I. The measured ZFS voltage spacings for different stack lengths.

Length	ZFS1	ZFS2	ZFS3
40 μm	0.855 mV		
60 μm		1.110 mV	
80 μm		0.825 mV	1.225 mV

fact that $L=20\,\mu$m stack is not in the long junction limit (especially, for in-phase mode), we exclude it from further consideration.

The voltage of the kth in-phase ZFS in a twofold stack is given by the expression

$$V_k=2\Phi_0\frac{\overline{c}_+}{L}k, \quad k=1,2,3\ldots \quad . \tag{12}$$

The factor of 2 on the right-hand side (RHS) of the expression appears because the voltage of the synchronized ZFS is measured across the whole stack. We observed one ZFS for the stacks with $L=40,60\,\mu$m and two ZFS's for $L=80\,\mu$m. The voltages of the steps are summarized in Table I. Now, we have to understand which step of order k we observed for different lengths. Expressing the Swihart velocity $\overline{c}_+$ from Eq. (12) as

$$\overline{c}_+=\frac{LV_k}{2k\Phi_0}, \tag{13}$$

we have to choose the integer k for each of the four steps in such a way that we get (with high accuracy) the same value of $\overline{c}_+$ for all three stacks. This technique gives $k=1$ for the $L=40\,\mu$m stack, $k=2$ for the $L=60\,\mu$m stack, and $k=2$ and 3 for the $L=80\,\mu$m stack. The calculated Swihart velocity for these values of k is

$$\overline{c}_+=(0.027\pm0.00046)c \tag{14}$$

(relative error $\pm2\%$), where c is the speed of light in vacuum.

Up to this point, we had not proved that the observed ZFS's are indeed in-phase $\overline{c}_+$ ZFS's. To prove that, we measured the spacing between FS's of a single JJ in the stack. The measurements were performed in the voltage range $V>|\Delta_{a,b}+\Delta_m|/e$ at $T=4.2$ K. This range was chosen to make sure that one JJ is at the gap sum voltage $|\Delta_{a,b}+\Delta_m|/e$ and the resonances take place only in the other JJ. An example family of IVC's, recorded using a digital oscilloscope while sweeping a magnetic field, is shown in Fig. 6 for the $L=60\,\mu$m stack. The applied magnetic field H was varied in the range 10–35 Oe. A similar picture (though with different voltage spacings between FS's) was observed for the stacks with $L=40,80\,\mu$m. The FS voltage spacings can be expressed as

$$\Delta V=\Phi_0\frac{\overline{c}_-}{2L}. \tag{15}$$

It depends on L, therefore, to compare stacks of different lengths we express $\overline{c}_-$ from Eq. (15):

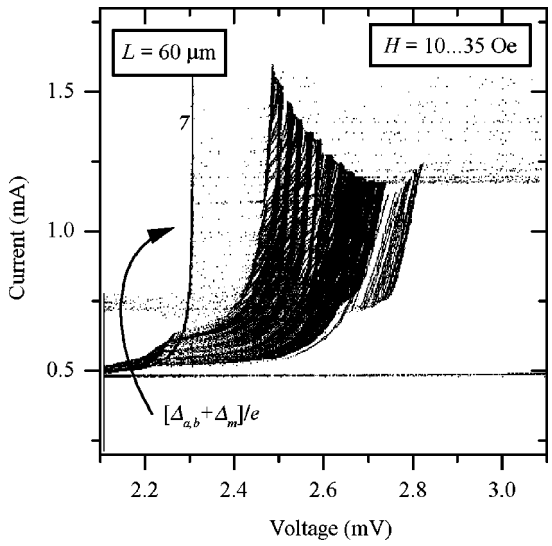

FIG. 6. The family of the Fiske steps observed above the gap voltage of a single JJ for the stack with $L=60\,\mu$m.

$$\overline{c}_-=\frac{2L\,\Delta V}{\Phi_0}. \tag{16}$$

The value for $\overline{c}_-$ calculated from the spacings of FS families for $L=40,60,80\,\mu$m is

$$\overline{c}_-=(0.0044\pm0.00018)c \tag{17}$$

(relative error $\pm4\%$). Swihart velocities given by Eqs. (17) and (14) are consistent with the fact that $\overline{c}_-$ should be less than $\overline{c}_+$. The ratio is

$$\frac{\overline{c}_+}{\overline{c}_-}=6.09\pm0.37 \tag{18}$$

(relative error $\pm6\%$). From Eqs. (18) and (5) the coupling strength is

$$S=-\frac{(\overline{c}_+/\overline{c}_-)^2-1}{(\overline{c}_+/\overline{c}_-)^2+1}=0.947\pm0.001 \quad (\pm0.1\%), \tag{19}$$

which is the highest known coupling strength between JJ's. Both $\overline{c}_+/\overline{c}_-$ and S are important parameters which characterize the inductive coupling strength. In the limit of very strong coupling ($S\lesssim1$) it is more convenient to use $\overline{c}_+/\overline{c}_-$ instead of S. Now, we have to check how well the value (18) fits the theory[10] by means of its comparison with the value calculated from the electrodes thicknesses.

The crucial point in the evaluation of the coupling from the experimental parameters is to take the right value for the London penetration depth λ_m of the very thin middle Nb-Al superconducting layer. To estimate this value, we use the relation [see Eq. (A17) from Appendix A]

$$\lambda_m\propto\frac{\sqrt{\rho}}{\Delta_m}, \tag{20}$$

where ρ is the normal resistivity of the middle superconducting film above T_c^m. Thus, both the resistivity and the energy gap of the film can affect the London penetration depth.

First, we evaluate the energy gap Δ_m at a working temperature from the experimental data shown in Figs. 3 and 4. In the calculations below, we assume that the energy gap of a superconductor depends on the temperature according to the empirical formula[18]

$$\Delta\left(\Delta_0, \frac{T}{T_c}\right) = \Delta_0 \sqrt{\cos\left[\frac{\pi}{2}\left(\frac{T}{T_c}\right)^2\right]} \tag{21}$$

From the position of step 6 in Fig. 3, using Eqs. (7) or (8) we have

$$2\Delta\left(\Delta_0, \frac{T_w}{T_c}\right) = V_6(T_w)e, \tag{22}$$

where $\Delta_0 = 1.4$ meV is the energy gap of the top and bottom electrodes at $T=0$, $T_c = 8.6$ K is their critical temperature measured in the separate experiment, and T_w is the working temperature at which the data shown in Fig. 3 were obtained. From the position of step 8 in Fig. 3, using Eqs. (9) and (22), we have

$$V_6(T_w)e + 2\Delta\left(\Delta_m(0), \frac{T_w}{T_c^m}\right) = V_8(T_w)e. \tag{23}$$

From Fig. 4 we obtain the third equation for the temperature T_c^m at which steps 5, 6, and 8 coincide with each other:

$$2\Delta\left(\Delta_0, \frac{T_c^m}{T_c}\right) = V_{5,6,8}(T_c^m)e. \tag{24}$$

Substituting

$$V_6(T_w) = 2.68 \pm 0.04 \text{ mV}, \tag{25}$$

$$V_8(T_w) = 4.20 \pm 0.15 \text{ mV}, \tag{26}$$

$$V_{5,6,8}(T_c^m) = 2.36 \pm 0.01 \text{ mV}, \tag{27}$$

into Eqs. (22)–(24), we solve the system of nonlinear equations (22)–(24) for T_w, T_c^m, and $\Delta_m(0)$ and obtain the following solution:

$$T_w = 4.40 \pm 0.36 \text{ K}, \tag{28}$$

$$T_c^m = 6.06 \pm 0.03 \text{ K}, \tag{29}$$

$$\Delta_m(0) = 0.79 \pm 0.11 \text{ meV}. \tag{30}$$

The values in Eqs. (28)–(30) were obtained by averaging over all four stacks. Using Eq. (21) we get

$$\Delta_m(T_w) = 0.76 \pm 0.12 \text{ meV} \tag{31}$$

(relative error $\pm 16\%$). $\Delta_m(T_w)$ can be also found by measuring steps 2 and 7 in Fig. 3. These steps are at the voltages $V_2 = (\Delta_{a,b} - \Delta_m)$ and $V_7 = (\Delta_{a,b} - \Delta_m)$, respectively. From these values we calculated $\Delta_m(T_w) \approx 0.7$ meV which coincides with Eq. (31) within the experimental error range.

The resistivity of rather thick ($d_s > 50$ nm) Nb films according to different data[19] is in the range

$$\rho_{\text{bulk}}(10\text{ K}) = 3.0 \pm 0.9 \ \ \mu\Omega \text{ cm}. \tag{32}$$

The resistivity of the epitaxial 7 nm Nb films grown on a sapphire substrate varies from 8.75 to 17.5 $\mu\Omega$ cm.[20] The Nb film in the middle electrode of our stack is granular and grew up on amorphous Al_2O_3. Thus, it would be rather realistic to take $\rho_{7\text{ nm}}(10\text{ K}) > 20\ \mu\Omega$ cm.

Finally, substituting this value of $\rho_{7\text{ nm}}$ and the value of $\Delta_m(T_w)$ from Eq. (31) into Eq. (20) we get

$$\lambda_m = \lambda_{a,b}\frac{\Delta_{a,b}}{\Delta_m}\sqrt{\frac{\rho_{7\text{ nm}}(10\text{ K})}{\rho_{\text{thick}}(10\text{ K})}} \approx 200 \pm 60 \text{ nm}. \tag{33}$$

To calculate the numerical value of λ_m in Eq. (33) we took $\Delta_m = 0.75$ meV which is very close to the value given by Eq. (30). The $\rho_{7\text{ nm}}(10\text{ K})/\rho_{\text{bulk}}(10\text{ K})$ ratio was chosen to be equal to 10. The exact value of this ratio is not very critical since it enters in Eq. (33) under the square root. From Eq. (33), the ratio $\overline{c}_+/\overline{c}_-$ can be calculated. Due to the fact that we do not know the exact value of $\rho_{7\text{ nm}}(10\text{ K})$ for our films, we use $\lambda_m\ [\rho_{7\text{ nm}}(10\text{ K})]$ as an adjustable parameter in the range specified above Eq. (33) in order to explain the value of $\overline{c}_+/\overline{c}_-$ calculated from the experimental data using Sakai-Bodin-Pedersen (SBP) theory.[10] This approach gives $\overline{c}_+/\overline{c}_- = 6.09$, Eq. (18), for

$$\lambda_m = 220 \text{ nm}, \quad \rho_{7\text{ nm}}(10\text{ K}) = 28 \pm 3\ \mu\Omega \text{ cm}. \tag{34}$$

Calculating the ratio $\overline{c}_+/\overline{c}_-$ above, we neglected the fact that the middle electrode is an Al-Nb bilayer and assumed that it is all Nb with suppressed gap. Since the thicknesses of Nb and Al layers are nearly equal, in the next section we will take into account the presence of Al film and see how this affects the result (34).

Since $d_{\text{Nb}} \ll \xi_{\text{Nb}}$ and $d_{\text{Al}} \ll \xi_{\text{Al}}$, the order parameter and the energy gap Δ_m are assumed to be constant (due to the proximity effect) along the z direction in the whole Nb-Al electrode. Since $\rho^{\text{Al}}(10\text{ K}) < \rho^{\text{Nb}}(10\text{ K})$ from Eq. (33) it follows that the penetration depth $\lambda_{\text{Al}} < \lambda_{\text{Nb}}$. Thus, the Al film screens magnetic field better than the Nb film. This increases the overall screening effect of the middle electrode and should result in a weaker coupling, i.e., a lower $\overline{c}_+/\overline{c}_-$ ratio. To take into account this effect, in the following section we extend SBP theory[10] for the case of twofold stacks with a middle electrode consisting of two different superconductors with London penetration depths λ_n (Al) and λ_s (Nb).

IV. EXTENSION OF THE SBP MODEL

We consider the twofold stack shown in Fig. 1. Following Ref. 10, we derive the equations for the superconducting phase difference in the two coupled JJ's, where the middle electrode consists of two different superconductors with London penetration depths λ_n (proximized Al) and λ_s (Nb). The z axis is directed perpendicular to the plane of the junc-

tion so that $z=0$ corresponds to the boundary between Nb and Al films and the middle electrode occupies the space from $-d_s$ to d_n.

If we have magnetic fields B_a and B_b in top and bottom JJ's, the magnetic field distribution in the middle Nb-Al electrode can be derived from the London equations as

$$B_s(z)=A\cosh(z/\lambda_s)+B\sinh(z/\lambda_s), \tag{35}$$

$$B_n(z)=A\cosh(z/\lambda_n)+\frac{\lambda_n}{\lambda_s}B\sinh(z/\lambda_n), \tag{36}$$

where $B_{n,s}(z)$ are local magnetic field in N (Al) and S (Nb) parts of the middle electrode:

$$A=\frac{\sinh(d_s/\lambda_s)B_a+r_{ns}\sinh(d_n/\lambda_n)B_b}{\cosh(d_n/\lambda_n)\sinh(d_s/\lambda_s)+r_{ns}\sinh(d_n/\lambda_n)\cosh(d_s/\lambda_s)}, \tag{37}$$

$$B=\frac{\cosh(d_s/\lambda_s)B_a-\cosh(d_n/\lambda_n)B_b}{\cosh(d_n/\lambda_n)\sinh(d_s/\lambda_s)+r_{ns}\sinh(d_n/\lambda_n)\cosh(d_s/\lambda_s)}. \tag{38}$$

$d_{n,s}$ and $\lambda_{n,s}$ are the thicknesses and London penetration depths of the proximized normal (Al) and superconducting (Nb) parts of the middle electrode, respectively; $r_{ns}=\lambda_n/\lambda_s$. The coefficients A and B are chosen to satisfy the boundary conditions

$$B_s(-d_s)=B_b,\quad B_n(d_n)=B_a,\quad \text{and } j_s(-0)=j_n(+0). \tag{39}$$

Now we have to calculate the current flowing on the top and bottom surface of the middle electrode, calculating a derivative of Eqs. (35) and (36) at $z=-d_s$ and $z=d_n$, respectively. The expressions obtained for the currents we put into Eq. (4) of Ref. 10 and after long but trivial simplifications we end up with the following [compare with Eq. (13) or (19) of Ref. 10]:

$$\frac{\Phi_0}{2\pi\mu_0}\frac{\partial^2}{\partial x^2}\begin{pmatrix}\phi^a\\ \phi^b\end{pmatrix}=\begin{bmatrix}d_a'' & r_{ns}^2 s_m\\ s_m & d_b''\end{bmatrix}\begin{pmatrix}J_Z^a\\ J_Z^b\end{pmatrix}, \tag{40}$$

where

$$d_a''=\lambda_a\coth\left(\frac{d_a}{\lambda_a}\right)+\lambda_n\frac{\tanh(d_n/\lambda_n)\tanh(d_s/\lambda_s)+r_{ns}}{\tanh(d_s/\lambda_s)+r_{ns}\tanh(d_n/\lambda_n)}, \tag{41}$$

$$d_b''=\lambda_b\coth\left(\frac{d_b}{\lambda_b}\right)+\lambda_s\frac{\coth(d_n/\lambda_n)\coth(d_s/\lambda_s)+r_{ns}}{\coth(d_n/\lambda_n)+r_{ns}\coth(d_s/\lambda_s)}, \tag{42}$$

$$s_m=\frac{-\lambda_s}{\cosh(d_n/\lambda_n)\sinh(d_s/\lambda_s)+r_{ns}\sinh(d_n/\lambda_n)\cosh(d_s/\lambda_s)}, \tag{43}$$

and $J_Z^{a,b}$ is the sum of all components of the current passing through the top and bottom JJ's, respectively. In the resistively shunted junction (RSJ) model,

$$J_Z^{a,b}=\frac{\Phi_0}{2\pi\mu_0}C^{a,b}\phi_{tt}^{a,b}+\frac{\Phi_0}{2\pi\mu_0}\frac{1}{R^{a,b}}\phi_t^{a,b}+J_c^{a,b}\sin(\phi^{a,b}). \tag{44}$$

One can easily check that if $\lambda_n=\lambda_s$ ($r_{ns}=1$), Eqs. (41)–(43) coincide with Eqs. (8a) and (8b) from Ref. 10.

The dimensionless coupling parameter S can be defined as

$$S=\frac{r_{ns}s_m}{\sqrt{d_a''d_b''}} \tag{45}$$

and is in the range $-1<S<0$. To obtain Swihart velocities, we consider the small-amplitude liner waves $\phi^{a,b}(x,t)=D_{a,b}e^{-j(kx-\omega t)}$ and, neglecting the term containing ϕ_t (damping) and linearizing the term $\sin\phi^{a,b}\approx\phi^{a,b}$ in Eq. (44), obtain

$$\frac{\overline{c}_+}{\overline{c}_-}=\sqrt{\frac{d_a''+d_b''+\sqrt{(d_a''-d_b'')^2+4S^2d_a''d_b''}}{d_a''+d_b''-\sqrt{(d_a''-d_b'')^2+4S^2d_a''d_b''}}}, \tag{46}$$

where we used the fact that

$$\overline{c}_\pm=\lim_{k\to\infty}\frac{\omega_\pm(k)}{k}.$$

As before, using λ_s as a free parameter and taking $\rho_s/\rho_n=5$ (i.e., $\lambda_n=\lambda_s/\sqrt{5}$) we get $\overline{c}_+/\overline{c}_-=6.1$ for $\lambda_s=215\,\text{nm}$. Expression (46) is rather sensitive to the value of λ_s; therefore, we can use it for an exact definition of λ_s from the ratio $\overline{c}_+/\overline{c}_-$ measured experimentally.

We can simplify the bulky expressions above taking into account that in our case $d_{n,s}\ll\lambda_{n,s}$ and assuming $\lambda_a=\lambda_b=\lambda$. In this limit, Eqs. (41)–(43) and (46) become

$$d_a''=\lambda\coth\left(\frac{d_a}{\lambda}\right)+\frac{\lambda_n^2}{d_n+d_s}, \tag{47}$$

$$d_b''=\lambda\coth\left(\frac{d_b}{\lambda}\right)+\frac{\lambda_s^2}{d_n+d_s}, \tag{48}$$

$$s_m=\frac{-\lambda_s^2}{d_n+d_s}, \tag{49}$$

$$\frac{\overline{c}_+}{\overline{\overline{c}}_-}=\sqrt{\frac{\lambda(d_s+d_n)+\lambda_s^2+\lambda_n^2}{\lambda(d_s+d_n)}}\approx\sqrt{\frac{\lambda_s^2+\lambda_n^2}{\lambda d_m}}. \tag{50}$$

We have to point out that in the limit $\lambda_n=\lambda_s$ ($r_{ns}=1$) Eqs. (40)–(50) are identical to conventional SBP (Ref. 10) equations. In particular, Eq. (50) becomes

$$\frac{\overline{c}_+}{\overline{\overline{c}}_-}=\sqrt{\frac{\lambda d_m+2\lambda_s^2}{\lambda d_m}}\approx\sqrt{\frac{2\lambda_s^2}{\lambda d_m}}. \tag{51}$$

From Eqs. (50) and (51) one may find a correction given by the extended theory (in the limit $d_{n,s}\ll\lambda_{n,s}$) in comparison with the regular SBP case:

$$\left(\frac{\overline{c}_+}{\overline{\overline{c}}_-}\right)_{\rm SBP}\Bigg/\left(\frac{\overline{c}_+}{\overline{\overline{c}}_-}\right)_{\rm ESBP}=\frac{\sqrt{2}}{\sqrt{r_{ns}^2+1}}\approx 1.3. \tag{52}$$

Thus, the extended SBP (ESBP) model gives a 30% correction to the SBP (Ref. 10) model. It is interesting that the final result does not depend on the thickness of the electrodes but only on the ratio $r_{ns}=\lambda_n/\lambda_s$.

V. CONCLUSION

We observed stable coherent ZFS's of the in-phase mode in strongly coupled stacked Josephson junctions. Both the critical current and the maximum ZFS current dependence on the magnetic field were measured. The dependences are in good agreement with the inductive coupling model proposed by Sakai *et al.*[10] The spacing of ZFS's in the $\overline{c}_+$ mode and Fiske steps in the $\overline{\overline{c}}_-$ mode is measured for different lengths of the stacks. In order to make a proper interpretation of the experimental results, an extension of the existing model[10] is developed. Our model takes into account the fact that the middle electrode consists of the two different superconductors (Nb and proximized Al). A comparison with the conventional model is made. It was found that for the case $d_{n,s}\ll\lambda_{n,s}$ the result obtained with our model differs by 30% from the conventional model and depends only on the ratio λ_n/λ_s.

ACKNOWLEDGMENTS

Funding of this work was provided by the Royal Society (UK) and by the INTAS program under Grant No. INTAS-94-1783.

APPENDIX A: CALCULATION OF THE LONDON PENETRATION DEPTH OF A VERY THIN Nb-Al ELECTRODE

In the structure under consideration the middle electrode is a proximity sandwich which consists of thin Nb and Al layers. The proximity effect in this electrode leads to a suppression of the effective gap in the density of states and an increase of the London penetration depth. To estimate these changes we will assume that both normal Al (N) and superconducting Nb (S) metals are in the dirty limit, and that their thicknesses d_n and d_s are smaller than the corresponding coherence lengths ξ_n and ξ_s,

$$d_n\ll\xi_n,\quad d_s\ll\xi_s, \tag{A1}$$

and the transparency of the SN interface is close to unity.

Under these assumptions we can start with the Usadel equations, which in our case have the form

$$\Delta\ln\frac{T}{T_c}+2\pi T\sum_\omega\left(\frac{\Delta}{\omega}-\frac{G_s\Phi_s}{\omega}\right)=0,\quad 0<z<d_s, \tag{A2}$$

$$\frac{D_s}{2\omega G_s}\frac{d}{dz}\left[G_s^2\frac{d}{dz}\Phi_s\right]-\Phi_s=-\Delta,\quad 0<z<d_s, \tag{A3}$$

$$\frac{D_n}{2\omega G_n}\frac{d}{dz}\left[G_n^2\frac{d}{dz}\Phi_n\right]-\Phi_n=0,\quad -d_n<z<0. \tag{A4}$$

Here $D_{s,n}$, $G_{s,n}=\omega/\sqrt{\omega^2+\Phi_{s,n}^2}$, and $\Phi_{s,n}$ are the diffusion coefficients and normal and anomalous Green's functions of the S and N materials, respectively; Δ is the order parameter of the S layer; $\omega=2\pi T(2n+1)$ are Matsubara frequencies; and T_c is the critical temperature of the bulk Nb. The z axis is oriented perpendicular to the interfaces of the structure. Equations (A2)–(A4) must be supplemented by appropriate boundary conditions matching the Green's functions at the SN interface,

$$\Phi_s(0)=\Phi_n(0),\quad \sigma_n\frac{d}{dz}\Phi_n(0)=\sigma_s\frac{d}{dz}\Phi_s(0), \tag{A5}$$

and at the boundaries with the insulating layers:

$$\frac{d}{dz}\Phi_n(-d_n)=0,\quad \frac{d}{dz}\Phi_s(d_s)=0. \tag{A6}$$

Under conditions (A1), to the first approximation, we can neglect the nongradient terms in (A3) and (A4) and get

$$\Phi_s=\Phi_n=A=\text{const}. \tag{A7}$$

Matching this solution with the one, which is easy to obtain in the high-frequency limit, we finally arrived at

$$\Phi_s=\Delta+(A-\Delta)\frac{\cosh[(z-d_s)/\xi_s]}{\cosh[d_s/\xi_s]}, \tag{A8}$$

$$\Phi_n=A\frac{\cosh[(z+d_n)/\xi_n]}{\cosh[d_n/\xi_n]}, \tag{A9}$$

where

$$A=\Delta\frac{\tanh[d_s/\xi_s]}{\tanh[d_s/\xi_s]+\gamma\tanh[d_n/\xi_n]}, \tag{A10}$$

$$\xi_{s,n}=\frac{D_{s,n}}{2\sqrt{\omega^2+A^2}}, \tag{A11}$$

$$\gamma=\frac{\rho_s\xi_s}{\rho_n\xi_n}. \tag{A12}$$

After substitution of the value of $\Phi_s(d_s)$, calculated from Eq. (A9), into the self-consistency equation (A2), we get the equation which determines the temperature dependence of the order parameter in the SN bilayer:

$$\ln\frac{T}{T_c}+2\pi T\sum_{\omega}\left(\frac{1}{\omega}-\frac{1-q(T)}{\sqrt{\omega^2+\Delta^2(1-q(T))^2}}\right)=0, \tag{A13}$$

$$q(T)=\gamma\frac{\tanh[d_n/\xi_n]}{\tanh[d_s/\xi_s]+\gamma\tanh[d_n/\xi_n]}\frac{1}{\cosh[d_s/\xi_s]}. \tag{A14}$$

Introducing the critical temperature of the SN sandwich $T_c^\star$ by putting $\Delta=0$ in Eq. (A13),

$$\ln\frac{T_c^\star}{T_c}+2\sum_{n}\left(\frac{1}{2n+1}q(T_c^\star)\right)=0, \tag{A15}$$

we can rewrite Eq. (A13) in the form

$$\ln\frac{T}{T_c^*}+2\pi T\sum_{\omega}\left(\frac{1-q(T_c^*)}{\omega}-\frac{1-q(T)}{\sqrt{\omega^2+\Delta^2[1-q(T)]^2}}\right)=0. \tag{A16}$$

Equations (A13)–(A16) together with the well-known expression for the London penetration depth λ,

$$\frac{1}{\lambda_{s,n}^2}=\mu_0\frac{4\pi T}{e\rho_{s,n}}\sum_{\omega}\frac{A^2}{\omega^2+A^2}, \tag{A17}$$

define the dependences of the penetration depths λ_s (for the Nb part) and λ_n (for the Al part) on temperature and material constants of the SN bilayer.

APPENDIX B: SIMULATION OF $I_{max}(H)$

In order to make a more complete comparison with theory, we performed numerical simulations of ZFS's for a strongly coupled two-junction stack. We employed the coupled sine-Gordon model developed by Sakai *et al.*[10] The model consists of a system of partial differential equations

$$\begin{cases}\dfrac{1}{1-S^2}\phi^a_{xx}-\phi^a_{tt}-\sin\phi^a=\alpha\phi^a_t-\gamma+\dfrac{S}{1-S^2}\phi^b_{xx},\\[2ex] \dfrac{1}{1-S^2}\phi^b_{xx}-\phi^b_{tt}-\sin\phi^b=\alpha\phi^b_t-\gamma+\dfrac{S}{1-S^2}\phi^a_{xx},\end{cases} \tag{B1}$$

with the boundary conditions

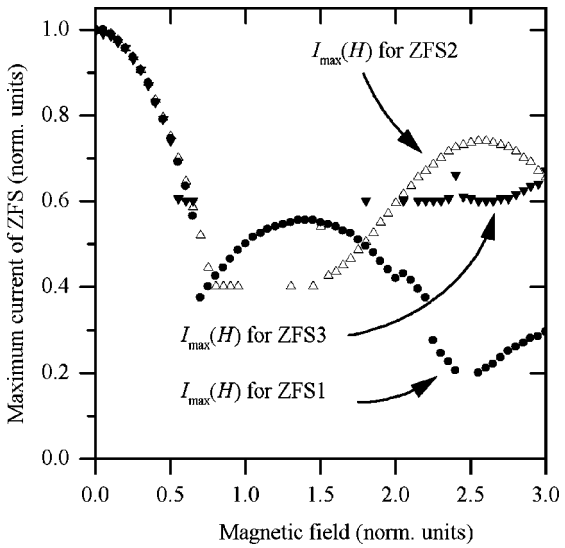

FIG. 7. Simulated dependence of the maximum current I_{max} of the steps $ZFS_{1,2,3}$ on applied magnetic field H. $\alpha=0.05$, $S=-0.9$, and $\ell=5$.

$$\begin{cases}\phi^a_x|_{x=0,\ell}=h,\\ \phi^b_x|_{x=0,\ell}=h.\end{cases} \tag{B2}$$

Equations (B1) are written in normalized units and, for simplicity, do not include the term $\beta\phi_{xxt}$, associated with the surface current losses. This so-called β term is relevant to the behavior of the system in the relativistic limit at temperatures far below T_c. Close to T_c, it is considerably smaller than the α-loss term arising from quasiparticle tunneling. The spatial coordinate x is normalized to λ_J. The time coordinate is normalized to the inverse plasma frequency $1/\omega_p$. For simulations we have used $S=-0.9$ and $\alpha=0.05$, which are close to the estimated values of the parameters in our experiments. The individual junction length was equal to $\ell=L/\lambda_J=5$, corresponding to $\ell_+=\ell\sqrt{1+S}\approx1.9$. We simulated ZFS's by starting from one, two, or three properly Lorenz-contracted fluxons inside each long Josephson junction, each fluxon moving with the same velocity u, close to, but less than $\overline{c_+}$. A driving current is supplied to support their motion. The simulated $I_c(H)$, $I_{max}^{ZFS_1}(H)$, $I_{max}^{ZFS_2}(H)$, and $I_{max}^{ZFS_3}(H)$ dependences are shown in Fig. 7. One can see that, similar to experiment, all curves have a maximum at $H=0$. In general, the dependence of the simulated step amplitudes accounts well for the single-junction case with renormalized length ℓ_+,[21] which is expected from the renormalized junction model for the coherent mode. As in experiment, there is a threshold current which limits the minimum $I_{max}^{ZFS}(H)$ which can be simulated. ZFS's cannot be suppressed by a magnetic field below the current $I_{min}=V_{ZFS}/R$. Thus, the experimentally observed $I_c(H)$ and $I_{max}^{ZFS_{1,2,3}}(H)$ dependences are in good agreement with inductive coupling model.[10]

*Permanent address: Institute of Radio Engineering and Electronics, Moscow, 103907, Russia.
Electronic address: gold@hitech.cplire.ru
†Permanent address: Institute for Nuclear Research, Moscow State University, 119899 GSP, Moscow, Russia.
‡Permanent address: Institute of Metal Physics, Ukrainian National Academy of Sciences, 252180 Kiev, Ukraine.
§Permanent address: Physikalisches Institut III, Universität Erlangen-Nürnberg, D-91058, Erlangen, Germany.
‖Permanent address: Department of Material Science and Metal-

lurgy, University of Cambridge, Cambridge, UK.
[1] M. G. Blamire, E. C. G. Kirk, J. E. Evetts, and T. M. Klapwijk, Phys. Rev. Lett. **66**, 220 (1991).
[2] H. Amin, M. G. Blamire, and J. E. Evetts, IEEE Trans. Appl. Supercond. **AS-3**, 2204 (1993).
[3] A. V. Ustinov, H. Kohlstedt, M. Cirillo, N. F. Pedersen, G. Hallmanns, and C. Heiden, Phys. Rev. B **48**, 10 614 (1993).
[4] I. P. Nevirkovets, J. E. Evetts, and M. G. Blamire, Phys. Lett. A **187**, 119 (1994).
[5] P. R. Auvil and J. B. Ketterson, J. Appl. Phys. **61**, 1957 (1987).
[6] A. V. Ustinov, H. Kohlstedt, and C. Heiden, Appl. Phys. Lett. **65**, 1457 (1994).
[7] I. P. Nevirkovets, Supercond. Sci. Technol. **8**, 575 (1995).
[8] E. D. Rippert, S. N. Long, J. B. Ketterson, S. R. Maglic, S. Lomatch, C. Thomas, M. A. Cheida, and M. P. Ulmer (unpublished).
[9] R. Kleiner, F. Steinmeyer, G. Kunkel, and P. Müller, Phys. Rev. Lett. **68**, 2394 (1992); R. Kleiner and P. Müller, Phys. Rev. B **49**, 1327 (1994).
[10] S. Sakai, P. Bodin, and N. F. Pedersen, J. Appl. Phys. **73**, 2411 (1993).
[11] E. Goldobin, A. Golubov, and A. V. Ustinov, Czech. J. Phys. **46**, 663 (1996).
[12] S. N. Song, S. Maglic, C. D. Thomas, M. Ulmer, and J. B. Ketterson, J. Appl. Phys. **80**, 2949 (1996).
[13] J. C. Swihart, J. Appl. Phys. **32**, 461 (1961).
[14] K. L. Ngai, Phys. Rev. **182**, 55 (1969).
[15] R. Monaco, A. Polcari, and L. Capogna, J. Appl. Phys. **78**, 3278 (1995).
[16] N. Grønbech-Jensen, D. Cai, and M. R. Samuelsen, Phys. Rev. B **48**, 16 160 (1993).
[17] H. Amin, M. G. Blamire, K. Page, and J. E. Evetts, IEEE Trans. Magn. **MAG-27**, 3145 (1991).
[18] T. P. Sheahen, Phys. Rev. **149**, 368 (1966).
[19] V. Lacquaniti, S. Maggi, E. Monticone, and R. Steni, Phys. Status Solidi A **151**, 335 (1995).
[20] K. Yoshii, H. Yamamoto, K. Saiki, and A. Koma, Phys. Rev. B **52**, 13 570 (1995).
[21] M. P. Soerensen, R. D. Parmentier, P. L. Christiansen, O. Skovgaard, B. Dueholm, E. Joergensen, V. P. Koshelets, O. A. Levring, R. Monaco, J. Mygind, N. F. Pedersen, and M. R. Samuelsen, Phys. Rev. B **30**, 2640 (1984).